Металлофиз. новейшие технол. / *Metallofiz. Noveishie Tekhnol.*
2018, т. 40, № 5, сс. 661–681 / DOI: 10.15407/mfint.40.05.0661
Оттиски доступны непосредственно от издателя
Фотокопирование разрешено только
в соответствии с лицензией

ФАЗОВЫЕ ПРЕВРАЩЕНИЯ

PACS numbers: 61.50.Ks, 61.72.Mm, 64.70.D-, 68.08.De, 68.70.+w, 81.10.Aj, 81.30.Fb

Non-Steady-State Growth During Directional Solidification of Various Crystallographic Orientations

O. P. Fedorov[*,***], V. F. Demchenko[**], and E. L. Zhivolub[***]

[*] *Space Research Institute, N.A.S. of Ukraine and State Space Agency of Ukraine, 40, 4/1 Academician Glushkov Ave., UA-03187 Kyiv, Ukraine*
[**] *E. O. Paton Electric Welding Institute, N.A.S. of Ukraine, 11 Kazymyr Malevych Str., UA-03150 Kyiv, Ukraine*
[***] *G. V. Kurdyumov Institute for Metal Physics, N.A.S. of Ukraine, 36 Academician Vernadsky Blvd., UA-03142 Kyiv, Ukraine*

The growth pattern in the thin and bulk samples of various crystallographic orientations is studied using direct observation of solid–liquid interface in transparent substances and microstructure of Al–Si single crystals. The evolution of regular tilted cells and split seaweed structures is observed in thin samples for different growth orientations and growth rates. During direct study in bulk samples, elongated cells appeared only for <110> orientations, whereas, for <100> orientations, only equiaxed cells appeared. This effect is associated with simultaneous development of the regular cell and irregular seaweed structures in single crystals with growth orientation different from <100>. Continuous pattern evolution due to the effect of solute accumulation results in non-steady-state interface propagation and transformation of elongated cells eventually into equiaxed ones.

Key words: solidification microstructures, crystallographic orientation, solid/liquid interface, cell and dendrite, heat and mass transfer.

Досліджено структури росту в тонких і масивних зразках різних кристалографічних орієнтацій шляхом прямого спостереження інтерфейсу тве-

Corresponding author: Yevhenii Leonidovych Zhyvolub
E-mail: zhivolub@imp.kiev.ua

Citation: O. P. Fedorov, V. F. Demchenko, and E. L. Zhivolub, Non-Steady-State Growth During Directional Solidification of Various Crystallographic Orientations, *Metallofiz. Noveishie Tekhnol.*, **40**, No. 5: 661–681 (2018), DOI: 10.15407/mfint.40.05.0661.

рде тіло–рідина у прозорих речовинах і мікроструктурі монокристалів Al–Si. Вивчалась еволюція реґулярних нахилених комірок і розщеплених структур «морські водорості» в тонких зразках для різних орієнтацій і темпів росту. Пряме спостереження об'ємних зразків показало, що витягнуті комірки з'являються лише для орієнтацій <110>, тоді як для орієнтацій <100> спостерігалися лише рівновісні комірки. Цей ефект пов'язаний з одночасним розвитком реґулярної коміркової та нереґулярної «водоростевої» структур у монокристалах з орієнтацією росту, відмінною від <100>. Безперервна еволюція зразка внаслідок ефекту накопичення розчину приводить до нестаціонарного розповсюдження інтерфейсу та перетворення витягнутих комірок у рівновісні.

Ключові слова: затвердіння мікроструктури, кристалографічна орієнтація, інтерфейс тверде тіло/рідина, комірка та дендрит, тепло- і масоперенесення.

Исследованы структуры роста в тонких и массивных образцах разных кристаллографических ориентаций путём прямого наблюдения интерфейса твёрдое тело–жидкость в прозрачных веществах и микроструктуре монокристаллов Al–Si. Изучалась эволюция регулярных наклонных ячеек и расщеплённых структур «морские водоросли» в тонких образцах для разных ориентаций и темпов роста. Прямое изучение объёмных образцов показало, что вытянутые ячейки появлялись только для ориентаций <110>, тогда как для ориентаций <100> наблюдались только равноосные ячейки. Этот эффект связан з одновременным развитием регулярной ячеечной и нерегулярной «водорослевой» структур в монокристаллах с ориентацией роста, отличной от <100>. Непрерывная эволюция образца вследствие эффекта накопления раствора приводит к нестационарному распространению интерфейса и трансформации вытянутых ячеек в равноосные.

Ключевые слова: затвердевание микроструктуры, кристаллографическая ориентация, интерфейс твёрдое тело/жидкость, ячейка и дендрит, тепло- и массоперенос.

(Received December 12, 2017)

1. INTRODUCTION

It is well known that the properties of crystalline materials are controlled by the microstructure that appears during solidification. Therefore, the morphology of solidification pattern is of practical importance because of its critical responsibility for the distribution of solute and defects in crystals. Commercial technologies of casting, welding, single crystal pulling from the melt are based on physical mechanisms of microstructure formation during directional solidification of binary alloy melts. The precise study of interface dynamics was successfully carried out using direct observation of solid–liquid

boundary evolution in transparent organic alloys. This method has been used for several decades and has provided information on stability loss of planar interface and pattern selection process. In generic experiment, the sample is pulling at a constant rate V through fixed temperature gradient G. When V exceeds a critical value, the interface becomes morphologically unstable as described by Mullins–Sekerka theory [1]. An unstable interface evolves into complex patterns of comprised cells, dendrites or seaweed and fractal-like structures.

Experimental studies have shown nonlinear dynamic phenomena that evolve after the onset of cellular growth (secondary instabilities): cell eliminations, tip splitting, one-side branch emission, cell oscillations, traveling waves, asymmetric cellular and dendritic doublets [2–6]. Temporal evolution of unstable interface is influenced by several factors, both intrinsic and extrinsic, specifically crystalline anisotropy, phase boundaries and subboundaries, dislocations, contacts with container walls, fluid flow modulations of the interface, *etc.* [7]. Further understanding of microstructure selection depends critically on the insight into these nonlinear phenomena.

One of the important dynamic factors that determine the selection process and the microstructure of crystalline material is the crystallographic anisotropy. In earlier studies [8, 9], it was shown that the crystallographic anisotropy of a small magnitude (typical for continuous growth) affects the orientation of the protrusions on the rounded crystal growing in a supercooled melt [8]. In the case of directional solidification in a quasi-two-dimensional specimen, tilted cells appear if the growing direction does not coincide with the direction of preferential growth of <100> [9]. A large number of studies that investigate the structure of tilted cells and dendrites have appeared lately [10–14].

The analysis of experimental data for succinonitrile-based alloys has led to the non-linear dependence of tilt angle on Peclet number [10, 11]. Tilted cells and dendrites emerge when crystallographic anisotropy competes with anisotropy of heat flow during directional solidification. The rotation of cells and dendrites from thermal gradient direction to the preferred growth direction <100> is associated with the change in the shape of the tip and appearance of side branches with the increase of primary spacing. The tilted growth results in morphological changes and thus changes in microsegregation in crystalline materials.

In case of large angles between thermal gradient and preferential growth direction, another type of morphology, seaweed microstructure, was observed in experiments on transparent substances and metal alloys [15–22]. The characteristic of seaweed is the successive and continuous splitting of the tips as a result of growing competition between preferred crystal growth direction and heat removal direction. Akarmatsu *et al.* [15] distinguished two types of seaweed patterns, one of which can be considered as a permanent regime when grains are

close to the {111} plane ('degenerate seaweed'); the 'stabilized seaweed' is unsteady and disordered at low pulling velocity. As the pulling velocity is increased, the solidification front undergoes a transition from seaweed to tilted dendrite. The numerical simulation evidenced that noise at the solid–liquid interface is a crucial factor to drive the transition to the seaweed since the noise destroys the stability of the growing tip [21].

Transformation of tilted cells and dendrites to tip-splitting seaweed pattern was observed mainly in quasi-two-dimensional specimens and 2*D* simulation. Meanwhile, a similar effect was also observed in bulk samples, in the case of a local disorientation of grains or uneven distribution of the temperature gradient [22]. It is expected that different crystallographic planes of a single crystal can also have a different structure.

Cellular and dendritic structures of bulk single crystals of different crystallographic samples were studied both on metallic and organic materials [23–26]. In Ref. [24], the formation of elongated cells on transversal sections for <110> orientation and of equiaxed cells for <100> was established during the study of Pb–Sb single crystals. The qualitative explanation of the different morphology of different crystallographic planes was given in Ref. [23]. This effect of growth orientation was tested in numerous experiments, some of which indicated the sequence of morphological pattern irrespective of growth orientation [25, 26]. It indicates the difficulty in identifying growth morphology of different crystallographic faces in bulk single crystal. Thus, the long-standing problem of the cellular growth for different orientations in bulk crystals remains open for directional solidification.

In order to elucidate the interface morphology dynamics of the different crystallographic directions, it is necessary to take into account non-steady-state conditions at the crystallization front, in particular, the process of the build-up of solute concentration before the interface. Warren and Langer model [27] has been compared with some experimental results; Motta *et al.* [28] has demonstrated that growth microstructure usually develops during the initial solidification transient, while the solute boundary layer is still growing.

Considering the effects of time-dependent solute accumulation, some stages of morphology evolution might not be observed depending on the time of the observation and the growth parameters. In other words, it is necessary to clarify whether the morphology of different planes is indeed different under the same conditions and what the role of non-steady-state processes is.

The above considerations were used in the experimental approach in this study. Relevant calculations of the non-steady-state heat and mass transfer processes have been performed using the experimental set-up parameters. To get an insight into the influence of a small magnitude of crystallographic anisotropy, seed single crystals of different crystallo-

graphic orientations were fabricated. In this case, thin and bulk (cylindrical) samples were used, and steady-state conditions were provided during the long-term observation of the solidification front.

2. EXPERIMENTAL PROCEDURE

The experimental study of the crystallization process was carried out using a binary system of succinonitrile–acetone (SCN–0.1% wt. Ac) and pivalic acid, which had been studied in detail before and allowed carrying out direct observations of the crystallization front under strictly controlled conditions [25, 29–31]. The initial substances of Aldrich Company were additionally purified by vacuum distillation, and the degree of distillation was determined by the change in the liquidus temperatures of test samples and the known diagram of state [30]. Both substances are characterized by a continuous growth mechanism from the melt, the difference in the anisotropy of surface energy reaching an order of magnitude (0.5% for succinonitrile and 5% for pivalic acid [29]).

Experiments with thin preparations were conducted in a standard Bridgman-type installation, providing growth rates in the range of 0.5–1.8 μm/s with the accuracy of 5% and the constant temperature gradient of 20 K/cm. The temperature of the heater and cooler (copper containers) provided with temperature-controlled water to accuracy 0.05 K. The preparation was placed in a sealed sample formed by round plane-parallel glass plates (thickness: 30 μm, the length of the zone: up to 8 cm, overall dimensions: $D = 10$ cm). The monitoring of the interface evolution was preceded by obtaining a seed <100> single crystal. Special attention was paid to the control of seed crystal <100> orientation along the plane of the sample using the measurement of dendritic-arms' length from the both sides of dendritic stem. To obtain other orientations (between < 100> and <110>), the sample was rotated around vertical axes.

The Bridgman technique for the study of solidification in cylindrical samples (Fig. 1) includes a gradient system, a sample with a transparent substance, a linear drive and an optical systems unit placed in a protective box fastened on a base stand. The gradient system consists of an electric resistive heater and a thermoelectric cylinder-shaped cooler based on a Peltier element fastened on the same axis as the specimen. An opportunity for a change of distance between them is provided. The controlled heater temperature range is 40–100°C. The controlled cooler temperature range is 0–20°C.

The maintenance of the cooler and heater temperature stability is not less than 0.05 K. The gradient device ensures the maximum value of the temperature gradient along the specimen length in the crystallization front zone being up to 50 K/cm. The sample is a cylindrical pipe with the maximum length of 200 mm made of glass and filled with a

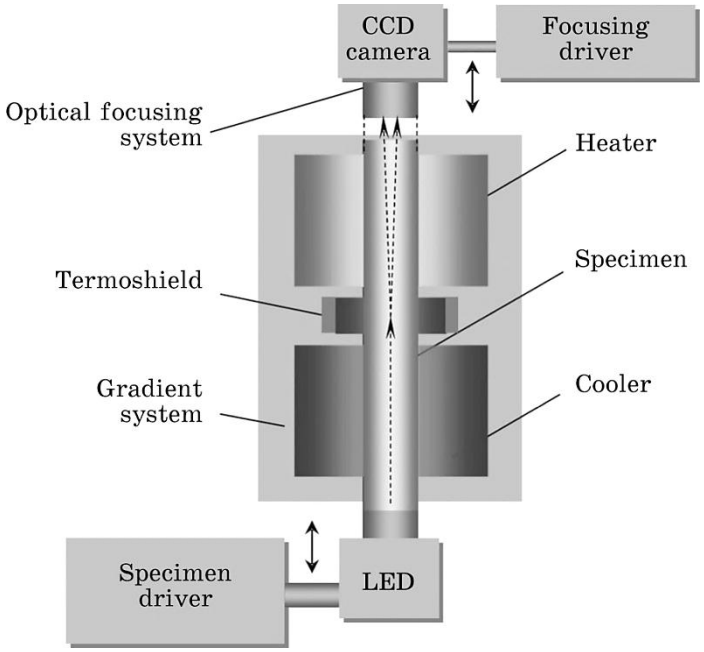

Fig. 1. A schematic drawing of the crystallization installation for bulk samples.

transparent substance. The linear drive moving velocity range is 0.1–30 μm/s in the working mode; the minimum moving velocity is 1 mm/s in the transport mode. The velocity maintenance accuracy is 5%.

The optical systems unit provides an image of the crystallization front and the adjacent crystal regions directly during the growth process. The unit includes a TV pickup camera, an image-focusing unit and illuminators. The image-focusing unit ensures both the static and dynamic image sharpness of the observed crystallization front, *i.e.* corrects the influence of the optical path change during the experiment. The optical system unit ensures the observation of the crystallization front through a molten substance zone along the specimen axis through a cuvette 'hot' end surface (providing its flatness).

The study of the influence of crystallographic orientation on the growth pattern is based on the utilization of seed single crystals of various orientations. Much attention was paid to the development of a technique for single crystal production. The orientation of a transparent single crystal was determined at the dendrite growth stage by the symmetry of its side branches arrangement against the dendrite stem. A profiled device for crystal growing, which allows changing growth direction of the initial crystal to a given angle, was used.

Direct comparison of thermal and concentration growth conditions is impossible, since the thermal parameters of metallic and organic

melts are significantly different. Nevertheless, one can qualitatively compare front morphology, considering that interface pattern evolution is similar (nodes, cells, cellular dendrites, dendrites). Metallic single crystals (diluted alloys of Al–Si) was grown using conventional Bridgman technique described in [32].

3. A NUMERICAL STUDY OF THERMAL AND DIFFUSION PROCESSES

One can restrict 2*D* approximation for both bulk and thin specimens, assuming that the temperature field of bulk specimen has axial symmetry and the temperature gradient across the width of the thin sample is negligible. In both cases, the heat propagation might be described by the thermal conductivity equation:

$$c\rho\frac{\partial T}{\partial t} = \frac{1}{x^n}\frac{\partial}{\partial r}\left(x^n\lambda\frac{\partial T}{\partial x}\right) + \frac{\partial}{\partial z}\left(\lambda\frac{\partial T}{\partial z}\right), 0 < x < L_x,\ 0 < z < L_z. \qquad (1)$$

Here, c, ρ are the specific heat and density of the material, λ is thermal conductivity, L_z is the length of the sample, $L_x = L + \delta_w$, δ_w stand for wall thickness, L is half-thickness of the thin sample (or the inner radius of the cylindrical specimen). The coordinate position x is the thickness of the thin preparation ($n = 0$), in the case of a cylinder ($n = 1$), the coordinate comes forward as the current radius. Considering the substantial difference in the thermophysical properties of succinonitrile and the glass of the ampoule, the wall of the ampoule is included in the area of solution of equation (1) that is integrated under the following boundary conditions:

$$\left.\frac{\partial T}{\partial z}\right|_{z=0} = 0,\quad \left.\frac{\partial T}{\partial z}\right|_{z=L_z} = 0,\quad \left.\frac{\partial T}{\partial x}\right|_{x=0} = 0,\quad \lambda\left.\frac{\partial T}{\partial x}\right|_{x=L_x} = \alpha[T(L_x, z, t) - T_c], \qquad (2)$$

where

$$\alpha(z,t) = \begin{cases} \alpha_g, & 0 < z < L_{hi}(t), \\ 0, & L_{hi}(t) < z < L_{ic}(t), \\ \alpha_g, & z > L_{ic}(t), \end{cases} \quad T = \begin{cases} T_{hi}, & 0 < z < L_{hi}(t), \\ T_{ic}, & z > L_{ic}(t), \end{cases}$$

$\alpha_g = \lambda_g/\delta$ is the coefficient of heat transfer through the gaseous gap; δ, λ_g stand for the thickness and thermal conductivity of the gas layer, $L_{hi}(t)$, $L_{ic}(t)$ stand for the current coordinates of the boundaries of the 'heater–insulator' and 'insulator–cooler'; T_{hi}, T_{ic} are the temperatures of the heater and the cooler, respectively. The heat flow on the border of the ampoule with an insulator was assumed zero.

In equation (1), the release of latent heat is negligible because, for

small pulling velocities (1–5 μm/s), it is much lower than the heat flux at the crystallization front. The equations (1), (2) were solved by means of finite-difference method using a five-point implicit difference scheme and numerical parameters corresponding to experimental conditions. The following parameters were used:

a) geometric dimensions: thickness of the plain preparation $L_p = 0.05$ cm (ampoule radius $R = 0.7$ cm for the bulk sample); thickness of the glass sample $L_g = 0.15$ cm; thickness of the air gap $\delta = 0.05$ cm; length of the sample $L_z = 10$ cm; the length of the insulator is 1 cm;

b) thermal parameters: thermal conductivity of the preparation $\lambda_p = 0.00220$ W/(cm·K); thermal conductivity of glass $\lambda_g = 0.0115$ W/(cm·K); specific heat capacity of solid phase $c_s = 1{,}08288$ J/(g·K); specific heat capacity of liquid phase $c_l = 1.49417$ J/(g·K); specific heat of glass $c_g = 0.8000$ J/(g·K); density of solid $\rho_s = 1.01600$ g/cm^3; melt density $\rho_l = 0.97510$ g/cm^3; melting temperature $T^* = 58$°C.

The temperature of the heater and the cooler as well as the thermal conductivity of the gas layer and the speed of pulling are varied.

The calculations of temperature distribution in the sample under different heater and cooler temperatures and pulling velocities exhibit the temperature field as sequence of stationary states corresponding to the different positions of the sample against the heater and the cooler. For this reason, it is possible to 'separate' the thermal and diffusion processes in the non-steady-state crystallization model of an alloy.

In the description of diffusion in binary alloy in thin specimen, the following assumptions were used: 1) the local thermodynamic equilibrium at the solidification front, *i.e.* the temperature and chemical composition of the coexisting phases corresponds to the equilibrium phase diagram of a binary alloy; 2) the temperature field in the melt is one-dimensional; 3) the crystallization front is flat; 4) the solute diffusion in the solid phase is negligible; 5) no melt flow.

The diffusion equation in the liquid phase ahead of the solidification front can be written as

$$\frac{\partial C}{\partial t} = D\frac{\partial^2 C}{\partial z^2}, \quad \xi(t) < z < L_0, \quad C(z,0) = C_0, \quad \xi_0 < z < L_0, \tag{3}$$

where $C(z, t)$ is the concentration of solute (acetone) in the liquid phase, C_0 is the initial concentration, D is the diffusion coefficient, L_0 is the length of the liquid phase prior to crystallization. At the crystallization front $z = \xi(t)$, the following condition for local mass balance is valid:

$$-D\left.\frac{\partial C}{\partial z}\right|_{z=\xi(t)} = \frac{d\xi}{dt}(1-\chi)C(\xi(t),t), \tag{4}$$

where χ is the distribution coefficient.

The solutions of equations (2)–(4) give the solute distribution values

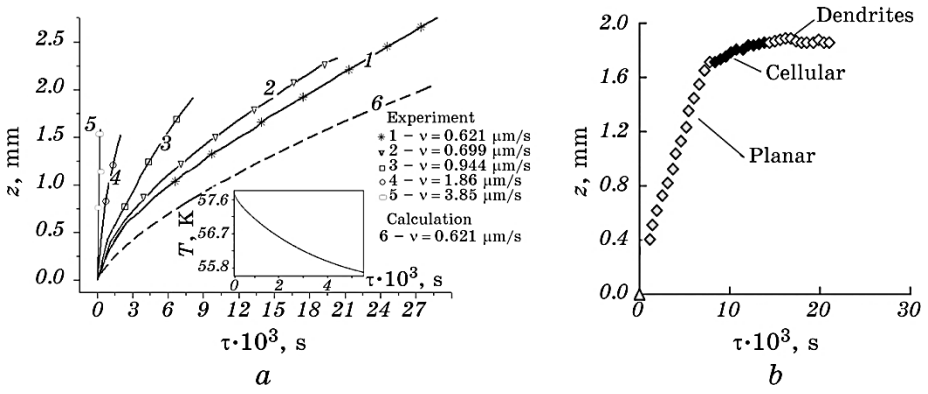

Fig. 2. Time dependence of the crystallization front position relative to the isotherm in thin specimen (front recoil, SCN + 0.1 Ac, <100>): various growth velocities; insert: change in crystallization temperature with time ($C_0 = 0.42\%$ wt. Ac, $v = 1.86$ μm/s) (*a*), $v = 1.86$ μm/s (*b*).

in the melt $C(z, t)$, $T_s(z, t)$, and the rate of crystallization $v(t)$. The results for T_s represent the sequences of identical temperature profiles, so temperature distribution hardly exerts any noticeable influence on observed dependence $z(t)$. At the same time, solute accumulation $C(z, t)$ and $T_s(t)$ are essentially time-dependent (Fig. 2, *a*) and appear to be the cause of the non-stationary front advancement.

The above calculations are valid only for planar interface and show a qualitative agreement with experiment (curve *1*, Fig. 2, *b*). A noticeable difference between the calculated and experimental values can be attributed to the influence of small amounts of uncontrolled impurities in SCN–0.1% Ac system.

4. EXPERIMENTAL RESULTS

4.1. Quasi-Two-Dimensional Samples. Front Recoil

In this work, the interface position was measured during the growth of planar, cellular and dendritic interfaces and compared (for planar front) with the calculations presented in the previous section. Experiments with all samples show front recoil (continuous drift backwards of the front position), whereas the effect depends on the speed of pulling and the interface morphology. When the interface is planar, the drift $z_0(\tau)$ is observed at a constant rate, the higher drift rate corresponding to the higher growth rate (Fig. 2, *b*). The development of cellular structure results in reduction of the recoil and its complete disappearance at the stage of deep cells and dendrites (Fig. 2, *c*). It should be noted that the data for the thin preparation are in qualitative

agreement with similar observations in the bulk sample and the relevant data in [28, 32].

The experimental data and relevant calculation for the planar interface are presented in Fig. 2, *b*. A numerical study aimed to elucidate the relative contribution of thermal and diffusion processes to observed non-steady-state effect of front recoil.

4.2. The Growth Pattern in Quasi-Two-Dimensional Samples

The sequence of growth patterns in thin sample (SCN–0.1% Ac and pivalic acid) for a fixed temperature gradient and different pulling rates

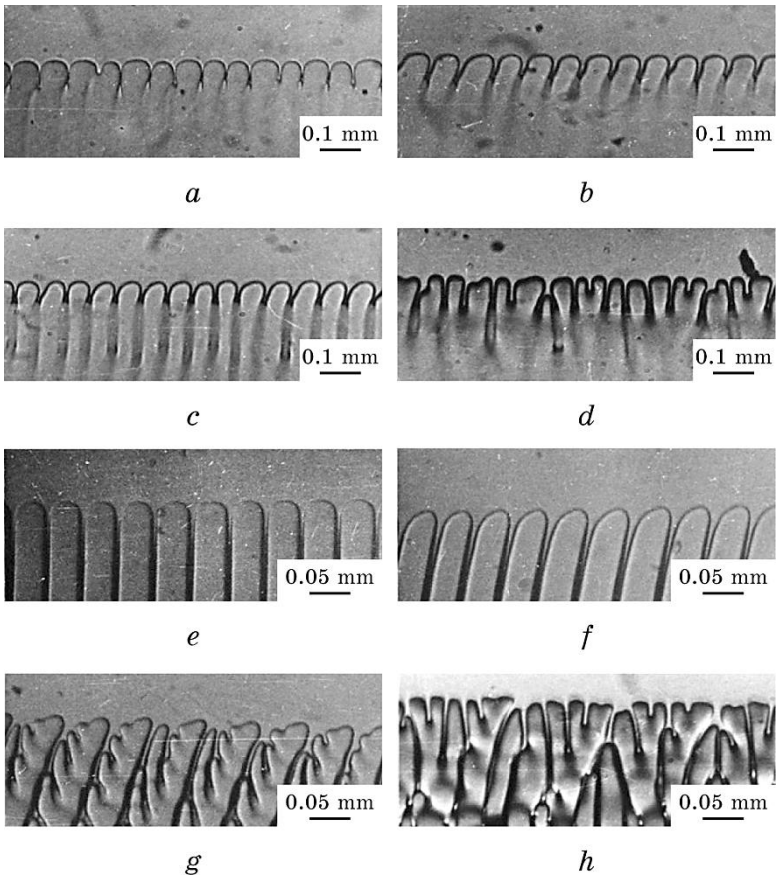

Fig. 3. Crystallization front morphology in thin samples for different orientations of SCN–0.1% wt. Ac single crystals: $\nu = 0.7$ μm/s (*a*–*d*), $\nu = 1.2$ μm/s (*e*–*h*). Angle between <001> and growing direction: 0° (<001>) (*a*, *c*, *e*), 20° (*b*, *f*), 30° (*c*, *g*), 45° (<110>) (*d*, *h*). Patterns in Fig. 3 were obtained in an experiment performed by A. Borisov.

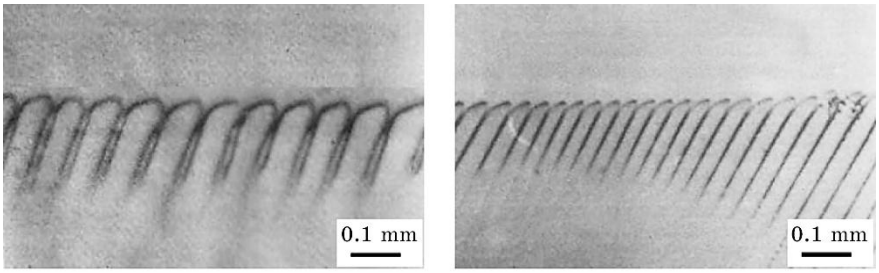

Fig. 4. Crystallization front morphology of <110> pivalic acid single crystals in thin sample: $v = 0.9$ μm/s (*a*), $v = 1.3$ μm/s (*b*).

and growth orientations is shown in Figs. 3, 4. If growth orientation is different from <100>, the interface morphology changes substantially.

The pattern of cellular evolution arises as a result of the deviation of growth direction from <100> and results in tilted cells or seaweed pattern. The structure formation may be indicative of competition between surface energy anisotropy and anisotropy effect related to the heat flow direction. The interface evolution for various orientations depends on growth rate as well on interfacial anisotropy.

In the region of cellular growth of SCN–0.1% Ac, the cells orientation is close to growth direction, whereas cell caps expand in <100> direction (Fig. 3, *a*–*c*). If growth direction coincides with <110> (misorientation angle up to 45 degree), permanent splitting appears (Fig. 3, *d*).

In the region of cellular dendrites, the periodically splitting growth pattern appears as the result of one-side branching (Fig. 3, *h*). It should be noted that the splitting pattern is the result of growing in <110> direction, whereas single crystals of orientations between <100> and <110> exhibit regular steady-state growth of tilted cells (cellular dendrites; Fig. 3, *e*–*g*).

Non-regular periodically splitting pattern for <110> single crystal (Fig. 3, *d*, *h*) was observed in the case of SCN–0.1% Ac in certain range of pulling velocities, corresponding to cells and cellular dendrites. Increasing the velocity causes the structure formed by tilted dendrites without signs of their splitting.

In the case of pivalic acid (and CBr_4–C_2Cl_6 system [33]), only regular tilted cells and dendrites are observed in the same range of growth parameters and <110> crystallographic orientations (Fig. 4; growth pattern for <100> is the same as shown in Fig. 3, *e*). It might evidence the critical importance of crystallographic anisotropy for the formation of regular morphology and steady-state growth for various crystal orientations (the anisotropy of succinonitrile surface energy is substantially lower than that of other two substances [29]).

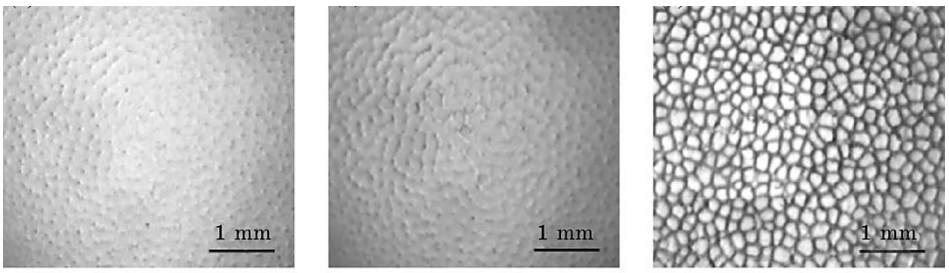

Fig. 5. Interface evolution during the growth of SCN–0.1% wt. Ac <100> single crystal in bulk sample.

5. BULK SAMPLES

5.1. Transparent Substances

The sequence of unstable structures arising at different growth rates of the succinonitrile <100> single crystal is shown in Fig. 5. Disturbance of the plane interface leads to the appearance of nodes—shallow depressions in the interface enriched with impurities. The sequence of growth patterns for the <100> orientation of succinonitrile (Fig. 5) and of pivalic acid is qualitatively close. The lack of node signs at the initial stage of stability loss for pivalic acid is noteworthy. The cause of the identified difference requires further investigation with the involvement of a wide range of materials with different anisotropy of surface energy (the data for node structure in metallic single crystals are contradictory and need more precise technique).

The further increase in growth velocity leads to the formation of grooves, most of which are initiated by the nodes (in the case of pivalic acid, the grooves appear spontaneously). The arrangement of grooves looks chaotic, but with time, the grooves transform into approximately regular honeycomb structure typical for equiaxed cells (Fig. 5, *b*, *c*).

It should be emphasized that no signs of elongated cells were recorded in any of the experiments with <100> single crystals. A fundamentally different picture of cellular structure formation is observed for <110> single crystals: developing grooves form the boundaries of elongated cells with time. Figure 6 represents the typical morphology for <100> and <110> single crystals of pivalic acid. It should be noted that both for succinonitrile and for pivalic acid, elongated cells are not completely ordered or geometrically regular. Intercellular boundaries are wavy lines; their elongation in one direction is much more distinct in pivalic acid that possesses higher crystallography anisotropy. Under constant growth conditions, elongated cells develop into equiaxed ones with time, in a little different from the respective morphology of

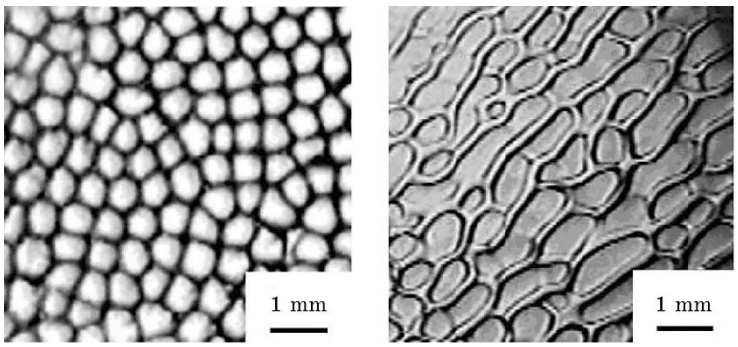

Fig. 6. Typical morphology of pivalic acid single crystals of <100> (*a*) and <110> (*b*) growth orientations.

<100> direction. Thus, elongated cells are registered as a stage of non-steady-state patterns in a certain range of rates. The higher the growth rate, there is the shorter this stage. No elongated cells are recorded for succinonitrile starting with the rate of 1.3 μm/s, and for pivalic acid—starting with the rate of 0.7 μm/s.

Succinonitrile <113> single crystals as well as those with orientations deviating from it at angles of up to 10° demonstrate the morphological sequence identical to that observed in <110> single crystals. The difference consists in the clearness of manifestation of the elongated cells, which, in the case of high-index directions, are present in the structure in the form of a geometrical motive, and poorly defined structural elements.

The above patterns were observed for single crystals in which the interface does not contain grain boundary or subboundary. In perfect single crystal, grooves appear and develop chaotically. Subboundaries (and grain boundaries in polycrystals), if they exist, initiate the ridges, aligned along a subboundary. This effect is observed and discussed in details in [34, 35]. Subboundaries are a constant source of ridges, so the relevant pattern can be taken for elongated cells. It seems to be the reason why in <100> single crystals such cells might be taken as elongated ones.

5.2. Metallic Single Crystals

A detailed description of metallic single crystals (Ni–Fe and Zn–Sn) of various orientations was presented in our previous work [36]. In this paper, the results for Al–Si single crystals grown using Bridgeman method described in Ref. [36] are presented.

For all the orientations of Al–Si single crystals, nodes appear as the

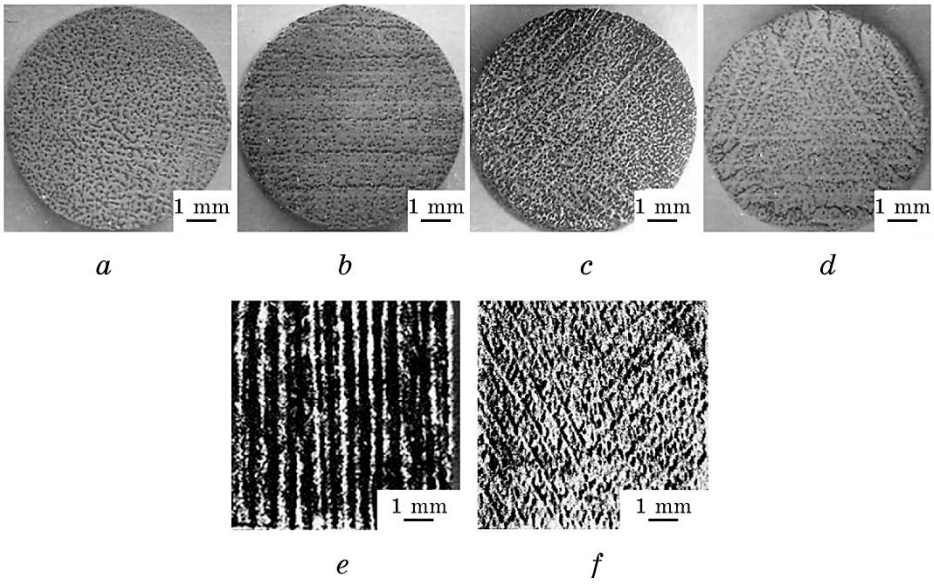

Fig. 7. Transversal (*a*–*d*) and longitudinal (*e*, *f*) sections of Al–Si single crystals shown on Fig. 8: <100> (*a*), <110> (*b*), <113> (*c*), <111> (*d*) single crystals, (001), (110) sections of <110> single crystal (*e*, *f*).

initial stage of planar interface stability loss. At higher growth rates, the cellular structure for single crystals of different orientations is fundamentally different. Microstructures of transversal sections of single crystals have traces of cells growing in a direction close to <100> (Fig. 7, *a*–*d*). Longitudinal sections of <100> single crystals both for (100) and (010) planes consist of solid intercellular lines, which is a manifestation of the rod-like structure of the <100> bulk crystal. In the case of the <110> single crystal, longitudinal section (110) consists of detached split elements (Fig. 7, *f*), whereas the (100) section demonstrates solid ones (Fig. 7, *e*). Therefore, the difference in the segregation structure of different single crystals is due to the different growth morphology of the cells in different orientations, which is illustrated in Fig. 8. It should be noted that cell brunching structure for (100) section of <110> single crystal is similar to the pattern for <110> succinonitrile single crystal (Fig. 3, *g*). The further increase in growth velocity results in dendritic structure, so all sections consist of solid elements (dendrites) growing in the <100> direction.

6. DISCUSSION

A direct observation of pattern formation dynamics using transparent single crystals and the microsegregation structure of metallic single

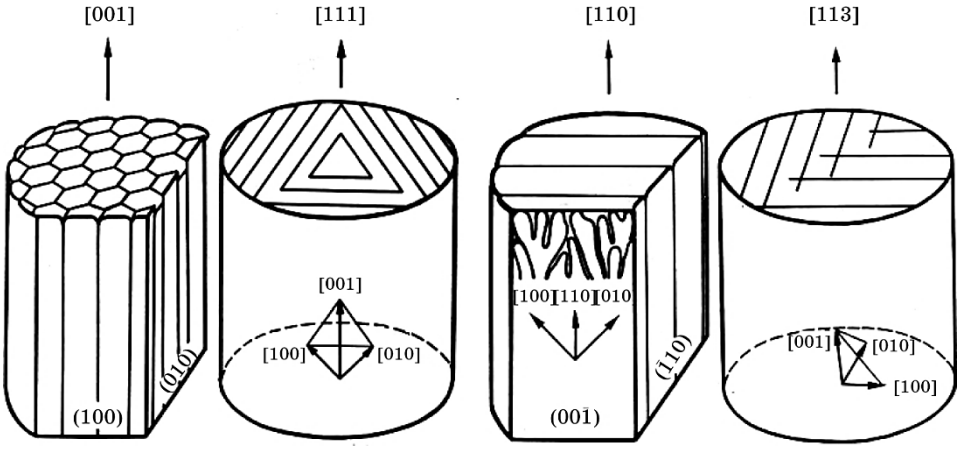

Fig. 8. Growth structure of Al–Si single crystals of various orientations.

crystals makes it possible to get an insight into some of the morphological features associated with unstable interface during directional solidification. The present study focused on the effects of crystallographic anisotropy (intrinsic) and solute accumulation before interface (extrinsic). Other known factors, which disturb the interface, were tried to be avoided or minimized: perfect single crystals without grains and subgrains were used; gravitational convection in a thin sample was significantly suppressed; crystallographic orientation of the single-crystals <100> is coincident with the plane of the sample to reduce the influence of the sample walls on the interface evolution.

The comparison of the data on organic and metal alloys has clear limitations because of the significant difference in heat and mass transfer in melts of these objects, but the morphological features of the evolution of the phase boundary are qualitatively similar, that repeatedly has been demonstrated in many studies, starting with basic research by Jackson and co-workers [37].

One of the most significant morphological effects observed in the transparent model alloys is associated with the different growth patterns for different crystallographic directions. Figure 3 demonstrates different options for cells evolution in quasi two-dimensional samples. Note that, in all experiments, crystallographic axis <100> coincides with the plane of the sample. Observation of different orientations was provided by rotating a plane single-crystal sample at different angles with respect to the direction of the temperature gradient. In other words, the interval of crystallographic directions that lie in one plane [110] in the range between <100> and <110> was studied.

Under typical growth conditions, the pivalic acid and CBr_4–C_2Cl_6 [33] having high value of surface energy anisotropy exhibits only tilt-

ed cells (cellular dendrites). Both shallow and deep cells have no indication of splitting even in the case of <110>.This does not mean that such a structure cannot be observed in principle. The experimental set-up does not allow changing the temperature gradient over a wide range, so it is not possible to achieve isotropic conditions at the interface.

Low-anisotropy SCN-based system exhibits a different pattern of cellular structure development, which depends both on the orientation and on the growth rate. Tilted cells are usually observed for growth direction misoriented with respect to <100> in the range of velocities corresponding to the transition from cells to dendritic cells. If growing direction makes an angle of more than 30 degrees with the direction <100>, cellular dendrites are formed with one-sided arrangement of the lateral branches under applied growth conditions. These side branches can catch up with the stem of a dendrite, and if the angle is equal to 45 degrees (direction <110>), the trunk and branches become indistinguishable.

At low velocities, the cells of SCN-based alloy are oriented in the direction of the heat flow, and their shape depends on the crystallographic direction. Competition of growth in preferred growth direction and heat flow direction leads to a flattening of the cell caps. When the directions of growth close to <110>, a branched structure appears consisting of periodically splitting elements (Fig. 3, *d*).

The branched microstructure (Figs. 3, *d* and *h*) seems to differ in the mechanism of formation and in the resultant of microsegregations. The first one (Fig. 3, *d*) is formed by continuously split cells symmetrically disposed relative to the growing direction, the second one (Fig. 3, *h*) is the result of one side brunching. In the first case, a practically isotropic microstructure appears, whereas the second mechanism results in fragments of oriented microstructure. Both types of seaweed pattern are 'compact structures' [22]; the pattern in Fig. 3, *j* corresponds to that obtained in [22] using phase field simulation. Meanwhile, one has never observed a detached seaweed with alternatively split asymmetrical brunches, which present simulation and observed experimentally ('stabilized seaweeds') [13, 21]. Such kind of structure appears in the case of arbitrary orientation of seed crystal relatively to plane of thin preparation (Fig. 9). Apparently, a detailed study of the interface morphology, taking into account the spatial distribution of the anisotropy of the surface energy, is needed to compose a complete picture of the various seaweed structures.

The microsegregation structure of Al-based single crystals of different orientations reveals a qualitative similarity with the structure of transparent single crystals. For instance, longitudinal sections (001) of <110> single crystal exhibit split microstructure, as cellular dendrites in Fig. 3, *h*. At the same time in (110) sections, only regular microstructure appears (Fig. 7, *e* and Fig. 8, *b*) as well as <100> single crystals

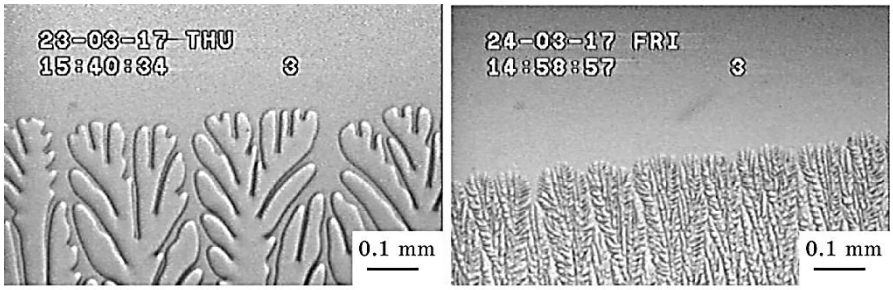

a *b*

Fig. 9. Interface morphology in thin sample of pivalic acid; crystallographic orientation<100> does not coincide with the plane of the sample: $v = 1.1$ μm/s (*a*), $v = 1.5$ μm/s (*b*).

demonstrate regular cellular structure in all longitudinal sections.

It is important to note that different types of microstructure appeared in different sections of the same single crystals. The above microsegregations schematically depicted in Fig. 8 can elucidate the origin of elongated and equiaxed cells formation. If preferred growth direction <100> inclined to the direction of growing, the competition between the crystallographic anisotropy and the heat flow anisotropy results in brunching pattern in certain interval of growth parameters.

Direct observations and microsegregation pattern of Al-based alloy strictly confirm the mechanism proposed in [23, 24]: for <100> single crystals, only equiaxed cells were observed, whereas elongated cells developed for orientation <110> (and <111>). The observed cell structure in a defect-free single crystal was formed because of the evolution of the grooves that had arisen spontaneously in the phase boundary. It is likely that the grooves propagation significantly differs for different crystallographic orientations of the phase boundary. It is worth noting that evolution of randomly distributed grooves to the ordered cell structure (elongated, equiaxed) is more clearly expressed for pivalic acid (Fig. 4), which has a higher anisotropy of surface energy.

Qualitatively, interface morphology is described by a scheme proposed in [23, 24]: equiaxed cells form with the <100> orientation, and elongated ones—with the <110> one. This scheme is consistent with experiments on metallic alloys, initially demonstrated by Morris and Winegard for Pb–Sb [24]. The transversal cross-sections of Al–Si single crystals exhibit the same sequence as the non-steady-state morphology as SCN–Ac (nodes, cells, cellular dendrites, dendrites).

Nevertheless, some authors consider elongated cells a stage in the development of the unstable interface structure (nodes, elongated cells and equiaxed cells) irrespective of growth orientation [26]. The authors of Ref. [4] observed no difference in the growth patterns of dif-

ferent orientations using the succinonitrile–acetone system and a bulk sample. In Ref. [25], a conclusion was made about the possibility of formation of elongated cells in <100> succinonitrile single crystals, the mechanism of their formation being associated with the impact of grain boundaries.

If the interface contains grain boundaries or subboundaries, the pattern evolution is more complicated because of interaction of grooves, ridges and boundaries described in details in [35]. In this case, observation of a cellular structure formation of different crystallographic directions is severely hampered. The use of single crystals allows to observe particular orientation of the phase boundary, as well as to assess the orientation of elongated cells. In all investigated <110>single crystals (both transparent and Al-based), elongated cells were stretched in the direction of <110>. It is worth to mention that the cells which look like elongated in <100> single crystals [25], have an arbitrary orientation, due apparently to the grain boundaries, which gave rise to them. These facts support the mechanism proposed in [23], which explains qualitatively the appearance of elongated cells by the surface energy difference for different slopes of distortion at the crystallization front.

A consistent description of elongated cells formation involves three-dimensional problems of stability loss of planar interface with the anisotropy of the surface energy taken into account. This work seems to contribute to the qualitative understanding description of cells formation, when growth direction does not coincide with the direction of preferential growth.

It is important that such a structure is essentially non-steady-state and transforms to a regular one under higher rates in the area of dendritic (cellular dendritic) growth.

Observation of elongated and equiaxed cells and calculations show that under typical solidification parameters of a succinonitrile-based transparent alloy, steady-state growth is not achieved. This effect is associated with time dependent solute accumulation before the interface, which is, in all probability, unavoidable under real experimental conditions with transparent organic substances Experiments with planar demonstrate the recoil of planar and cellular interface, and this effect depends on the speed of pulling. Figure 2, *b* shows that the smaller ν, the larger the value of displacement $z(t)$ and the length of the crystal, which has a planar solid–liquid interface. This fact leads to the conclusion that the applicability of the concept of 'critical growth velocity' is rather limited for actual growth conditions.

Another consequence of non-steady-state growth is the fact that elongated cells are observed in a certain range of growth parameters, being replaced with equiaxed ones, indistinguishable from the cells on the single crystal front <100>. In addition, elongated cells do not have

regular configurations due to their recurrent splitting and suppression. It is understandable that if elongated cells are manifested in a certain period of time, such experimental conditions exist when they are not found at all. This fact may explain the differences that occur when observing the evolution of the cellular structure in different studies.

7. CONCLUSIONS

1. Experimental observation of cellular interface evolution in thin samples for various crystallographic orientations exhibits the transformation of regular tilted cells to random splitting structure (seaweed morphology), when growth direction approaches <110>. This effect is strongly dependent on crystallographic anisotropy of the substance under study; split structures are characteristic for <110> SCN single crystal whereas pivalic acid <110> single crystals form only tilted cells under same growth conditions. This morphological effect emerges as a result of competitive processes due to anisotropy in surface properties of the interface and in heath–mass transport under directional pulling.
2. The branched seaweed microstructure depends on growth rate: under low rates (area of shallow cells) continuously split cells symmetrically dispose relative to the growing direction; in the region of deep cells, asymmetric one side brunching takes place. In the first case, isotropic microstructure appears, whereas the second mechanism results in fragments of oriented microstructure.
3. During bulk single crystal growing, both regular and split cellular structures appear in different cross-sections of the same crystal. In particular, for <110> Al-based single crystal, regular cells appear in longitudinal sections {111}, whereas, in sections {111}, irregular split morphology is observed. This effect occurs, when the preferential growth direction <100> (or its projection on the plane under consideration) does not coincide with the growing direction. Joint development of regular and irregular cell structure shows a complex spatial structure of the cells that develop in single crystals with growth orientation different from <100>. In particular, the formation of elongated cells in <110> single crystals (as well as certain other orientations) is explained by the interaction of regular and irregular structure arising in the bulk single crystal during growth in a direction different from the <100>.
4. During a direct study of growth pattern evolution for <100>, <110> and <111> succinonitrile single crystals in bulk samples, elongated cells were observed only for <110> and <111> orientations, whereas for <100>, only equiaxed cells appear. Because of continuous pattern evolution during the effect of non-steady-state interface propagation, elongated cells eventually transform into equiaxed ones and

their growth morphology becomes indistinguishable from that of <100> single crystals. Elongated cells are manifested in a certain period of time, so they are not observed at all under certain experimental conditions. Al-based single crystals of various orientations exhibit a growth pattern evolution similar to that observed in the succinonitrile transparent alloy.

The authors are grateful to A. G. Borisov for providing the experimental data shown in Fig. 3.

REFERENCES

1. W. W. Mullins and R. F. Sekerka, *J. Appl. Phys.*, **35**, No. 2: 444 (1964).
2. J. T. C. Lee and R. A. Brown, *Phys. Rev. B*, **47**, No. 9: 4937 (1993).
3. G. J. Merchant and S. H. Davis, *Phys. Rev. Lett.*, **63**, No. 5: 573 (1989).
4. S. de Cheveigne and C. Guthmann, *J. Phys. I France*, **2**: 193 (1992).
5. H. Jamgotchian, R. Trivedi, and B. Billia, *Phys. Rev. E*, **47**: 4313 (1993).
6. W. Losert, D. A. Stilman, H. Z. Cummins, P. Kopczyński, W.-J. Rappel, and A. Karma, *Phys. Rev. E*, **58**, No. 6: 7492 (1998).
7. M. Glicksman, *J. Cryst. Growth*, **450**: 119 (2016).
8. D. E. Ovsienko, A. M. Ovrutskii, and O. P. Fedorov, *ZhETF*, **73**, No. 3: 518 (1991).
9. A. G. Borisov, O. P. Fedorov, and V. V. Maslov, *J. Cryst. Growth*, **112**, Nos. 2–3: 463 (1991).
10. J. Dechamps, M. Georgelin, and A. Pocheau, *Europhys. Lett.*, **76**, No. 2: 291 (2006).
11. J. Dechamps, M. Georgelin, and A. Pocheau, *Phys. Rev. E*, **78**, No. 1: 011605 (2008).
12. A. Pocheau, J. Dechamps, and M. Georgelin, *Phys. Rev. E*, **81**, No. 5: 051608 (2010).
13. H. Xing, X. L. Dong, C. L. Chen, J. Y. Wang, L. F. Du, and K. X. Jin, *International J. Heat and Mass Transfer*, **90**: 911 (2015).
14. H. Xing, L. Zhang, K. Song, H. Chen, and K. Jin, *International J. Heat and Mass Transfer*, **104**: 607 (2017).
15. S. Akamatsu, G. Faivre, and T. Ihle, *Phys. Rev. E*, **51**, No. 5: 4751 (1995).
16. E. Brener, H. Müller-Krumbhaar, and D. Temkin, *Europhysics Lett.*, **17**, No. 6: 535 (1992).
17. E. Brener, H. Müller-Krumbhaar, and D. Temkin, *Phys. Rev. E*, **54**, No. 3: 2714 (1996).
18. T. Ihle and H. Müller-Krumbhaar, *Phys. Rev. Lett.*, **70**, No. 20: 3083 (1993).
19. B. Utter and E. Bodenschatz, *Phys. Rev. E*, **66**, No. 5: 051604 (2002).
20. A. Pocheau, J. Deschamps, and M. Georgelin, *JOM*, **59**, No. 7: 71 (2007).
21. Y. Chen, B. Billia, D. Zhjng Li, H. Nguen-Thi, N. Min Xiao, and A.-A. Bongo, *Acta Mater.*, **66**: 219 (2014).
22. M. Anoorezaei, S. Gurevich, and N. Provatas, *Acta Mater.*, **60**: 657 (2012).
23. M. Flemings, *Solidification Processing* (New York: McGrow-Hill Book Company: 1974).
24. L. R. Morris and W. C. Winegard, *J. Crystal Growth*, **5**: 361 (1969).
25. B. Kauerauf, G. Zimmermann, L. Murmann, and S. Rex, *J. Cryst. Growth*, **193**:

701 (1998).
26. A. A. Chernov, *Modern Crystallography III. Crystal Growth* (Ed. B. K. Vainshtein) (Berlin: Springer-Verlag: 1984).
27. I. A. Warren and J. S. Langer, *Phys. Rev. E*, **47**: 2702 (1993).
28. F. L. Mota, N. Bergeon, D. Tourret, A. Karma, R. Trivedi, and B. Billia, *Acta Mater.*, **85**: 363 (2015).
29. M. E. Glicksman and N. B. Singh, *J. Cryst. Growth*, **98**, No. 3: 277 (1989).
30. J. Lipton, M. E. Glicksman, and W. Kurz, *Mater. Sci. Eng.*, **65**, No. 1: 57 (1984).
31. R. Trivedi and K. Somboonsuk, *Acta Met.*, **33**, No. 6: 1061 (1985).
32. H. Jamgotchian, N. Bergeon, D. Binelli, P. Voge, and B. Billia, *J. Microscopy*, **203**, Iss. 1: 119 (2001).
33. O. P. Fedorov, *J. Cryst. Growth*, **156**: 473 (1995).
34. R. J. Schaefer and M. E. Glicksman, *Met. Trans.*, **1**: 1973 (1970).
35. N. Noel, H. Jamgotchian, and B. Billia, *J. Cryst. Growth*, **187**: 516 (1998).
36. E. L. Zhivolub and O. P. Fedorov, *Crystallogr. Rep.*, **43**: 139 (1998).
37. K. A. Jackson, D. R. Uhlmann, and J. D. Hunt, *J. Cryst. Growth*, **1**, No. 1: 1 (1967).